Journal of Applied Polymer Science

Physical, Mechanical, and Transdermal Diltiazem Release Analysis of Nanosilica Tailored Various Poly(vinyl alcohol) Membranes

Tridib Bhunia, Arindam Giri, Tanbir Nasim, Dipankar Chattopadhyay, Abhijit Bandyopadhyay
Department of Polymer Science and Technology, University of Calcutta, Calcutta 700009, India
Correspondence to: A. Bandyopadhyay (E-mail: abpoly@caluniv.ac.in)

ABSTRACT: Hybrid membranes based on poly(vinyl alcohol) (PVA) of widely different molecular weights and *ex situ* nanosilica were synthesized and characterized as transdermal delivery device for Diltiazem hydrochloride. Investigations showed that change in PVA molecular weight strongly influenced physico-mechanicals of the hybrids especially at low nanosilica content than at higher levels. As for example at 1 wt %, low molecular weight PVA induced finer dispersion of silica nanoparticles resulting into higher dry state crystallinity and mechanical strength but slightly lower biocompatibility as compared to high molecular weight PVA. Those variations in physico-mechanicals finally affected Diltiazem retention and its elution from those membranes under physiological conditions. Low molecular weight PVA produced highest drug retention as well as slowest yet steady release than both high molecular weight PVA and neat PVA membranes. © 2013 Wiley Periodicals, Inc. J. Appl. Polym. Sci. 000: 000–000, 2013

KEYWORDS: biodegradable; composites; drug delivery systems; membranes; gels

Received 31 October 2012; accepted 14 April 2013; Published online
DOI: 10.1002/app.39404

INTRODUCTION

Sustainable development in the field of controlled drug delivery is one of the major issues in medicinal biotechnology.[1–5] The delayed release maintains slow but steady drug concentration, which eventually reduces toxicity because of drug overload through multiple administrations and thereby improves patient compliance and comfort.[5–8] Various innovative routes related to control drug administration have been reported over the decades.[9–11] Delivery through skin or transdermal administration has been proved to be one of the most convenient methods particularly for those drugs that have low half life and generate severe side effects on prolonged intake. Diltiazem hydrochloride or simply Diltiazem is an important multipurpose drug of similar kind. It is an anti-anginal drug commonly prescribed to treat angina pectoris or chest pain.[12] It is also seldom prescribed for treating anal fissure.[13] As an anti-anginal drug, it belongs to the nondihydropyridine (nonDHP) category and acts by declining the oxygen demand of the heart. Its half life is only 3–4.5 h and produces fatal side effects like extremely low blood pressure and heart beat on regular intake. Unfortunately, patients suffering from such ailments are directed for prolonged Diltiazem intake. The drug is commercially marketed as 30, 60, 90, and 120 mg tablets. Intravenous formulation is also available for emergency. The recommended dose for an adult individual is 180 mg/day. The chemical structure of the drug is shown in Scheme 1. It is completely water soluble and the solution pH stays between 6.0 and 7.0.

Recently, polymer hydrogels have received much attention as controlled release device because of their unique potency to encapsulate several drugs and to restrict their elution without using any bioadhesive.[14–16] An ideal polymer patch must combine some unusual features such as, it must be soft and flexible (extensible) yet stronger (high modulus and strength), should absorb high amount of water (high swelling) to keep the underneath skin cool and, of course, should be permeable to air or oxygen. We have tried to achieve such odd combination of properties through different modifications of poly(vinyl alcohol) (PVA) as primarily, it forms stronger yet extendible hydrogel because of extensive intra and inter-molecular hydrogen bonding[17,18] and secondly, the membranes have excellent fitment with human skin regarding humidity and oxygen permeation properties.[19,20] Our previous investigation shows abrupt change in properties of PVA on changing its molecular weight but that excellently correlated with the Diltiazem release mechanism.[17,18]

There has been a lot of discussion on the effect of different nanomaterials on matrix polymer.[21–25] Generally, the nanoparticles improve physico-mechanicals of the matrix subject to their size, shape, and concentration. Such as addition of anisotropic carbon nanotube and clay to PVA achieved better mechanical, thermal, and electrical properties.[22,24] Similarly isotropic nano titanium dioxide (TiO_2) has improved thermal and mechanical properties of PVA such that it became suitable for direct methanol fuel cell application.[23] The present article

Applied Polymer SCIENCE

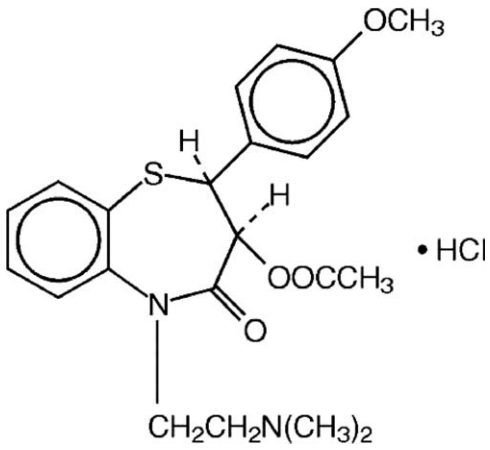

Scheme 1. Microstructure of diltiazem hydrochloride.

compares effect of *ex situ* nanosilica on dry- and wet-stage physico-mechanical, biocompatibility, and transdermal Diltiazem release kinetics under physiological condition between various PVA membranes. Isotropic nanosilica has surface silanol groups (Si-O-H) that produce strong hydrogen bonded interaction with PVA.[21,26] In addition, the aqueous sol is nontoxic, cheap, and solubilizes both PVA and Diltiazem molecules. To the best of our knowledge, not many studies have been carried out with *ex situ* nanosilica-PVA composite membranes using different PVAs. Also we are not aware of any previous studies on using such membranes as transdermal delivery device for Diltiazem delivery.

EXPERIMENTAL

Materials

PVA of widely different number of average molecular weights, 1.15×10^5 and 1.4×10^4, designated as PVA_H and PVA_L, with narrow molecular weight distribution (Polydispersity Index = 1.42) were purchased from Loba Chem, Mumbai, India. Aqueous nanosilica sol with 25% silica content and stabilized at pH 9.0, was generously supplied by Bee Chem, Kanpur, India. Sodium hydroxide, sodium lauryl sulphate, and buffer solution of pH 9.0, all of standard laboratory grades, were obtained from indigenous sources. Diltiazem hydrochloride, of molecular weight 450.98 was a gift sample received from Ranbaxy Int. Gurgaon, Haryana, India.

Membrane Preparation

A standard 10% (w/v) PVA solution was prepared by dissolving PVA in distilled water. Required amount of *N*/10 sodium hydroxide solution was added gradually to adjust the pH at 9. About 2.5 mL) standard buffer solution was added to arrest the pH. Nanosilica sol, premixed with 1% sodium lauryl sulphate, was mixed with PVA in different weight proportions under vigorous stirring and finally sonicated for 30 min. Different PVA–silica weight compositions are described in Table I. Composites that showed excellent physico-mechanical properties from each series were further synthesized with Diltiazem hydrochloride. In those cases, known weight of nanosilica sol was added to aqueous PVA sol premixed with 1 mg Diltizem and sonicated for 30 min. Hybrid nanocomposites were thinly cast over Teflon sheet and allowed for spontaneous drying in ambient. Accelerated drying was avoided to obtain defect free nanocomposite membranes. The average thickness of the free standing membranes was 0.25 mm.

Characterization of PVA–Silica Hybrid Membranes

Visual transparency of nanocomposite membranes were quantified in a UV–visible spectrophotometer, lamda 25 1.27 PerkinElmer, USA, within the visible range 600–700 nm. Atomic force microscope from Digital Instruments (Nanoscope III) and transmission electron microscope (C-12 Philips) operated at 120 kV were used to investigate the morphological aspects of hybrid membranes. X-ray silicon mapping of the membranes were recorded in an Oxford EDX system, attached to the scanning electron microscope, JEOL JSM 5800 to study nanosilica dispersion. The acceleration voltage was 20 kV. Swelling of hydrogel membranes was studied by putting samples in distilled

Table I. Sample Composition, Drug Diffusion Coefficient (k) and Release Exponent (n) Values of Different PVA–Silica Composite Membrane

Sample designation	PVA (%)	Nanosilica (wt %) w.r.t. PVA	Sodium lauryl sulphate (wt %) w.r.t. PVA	Net swelling ratio	k	n
PVA_H	10	0	0	7.03	10.83	0.436
$PVA_{H/0.5}$	10	0.5	1	4.79	-	-
$PVA_{H/1}$	10	1.0	1	4.33	1.27	0.937
$PVA_{H/2}$	10	2.0	1	4.16	-	-
$PVA_{H/3}$	10	3.0	1	3.89	-	-
$PVA_{H/5}$	10	5.0	1	3.55	-	-
PVA_L	10	0	0	4.55	8.71	0.491
$PVA_{L/0.5}$	10	0.5	1	7.52	-	-
$PVA_{L/1}$	10	1.0	1	4.78	1.79	0.894
$PVA_{L/2}$	10	2.0	1	3.83	-	-
$PVA_{L/3}$	10	3.0	1	3.63	-	-
$PVA_{L/5}$	10	5.0	1	3.49	-	-

water at room temperature (27 ± 2°C). After stipulated time interval, the samples were taken out of the water, gently wiped in tissue paper to soak surface water and finally weighed in an electronic balance (MK-20E, readability 0.1 mg Adair Dutt, India). The swelling ratio was calculated by dividing swelled weight (S) by dry weight (S_0) of the membranes. The experiment was carried out till the samples attained equilibrium. De-swelling experiment was done by periodically recording the decreasing weight of the fully swollen membranes in ambient air (27°C, RH: 85) till constant value was achieved. Wide angle X-ray diffraction (XRD) behavior of hydrogel membranes was studied in a X'pert PRO MRD X-ray diffractometer (PANalytical, The Netherlands) at room temperature (27 ± 2°C). The membranes were scanned at 2°/min between angles 10° and 35° at 45 kV with a current supply of 30 mA. Spectral data corresponding to both dry and wet membranes were taken and reproduced for analysis. Solid state ^{13}C nuclear magnetic resonance (NMR) spectroscopic analysis was done in a Bruker nmr spectrophotometer operated at 500 MHz under room temperature. Tensile stress–strain properties (tensile strength, modulus, and elongation at break) of dry and swelled hydrogel membranes were studied in a Lloyd UTM, USA, at room temperature (27 ± 2°C). The samples were cut using ASTM Die C from the membranes and were pulled at a rate of 10 mm/min. The samples were dumb-bell shaped having length 60 mm, breadth 10 mm, and depth 0.25 mm.

Biocompatibility, Drug Encapsulation Efficiency, and Transdermal Diltiazem Release Analysis

Biocompatibility was assessed by observing microbial growth over the physico-mechanically best hybrid membranes from each PVA series. The normal LB Agar-based media was prepared by mixing 10 g of Tryptone (E-Merck, Germany), 5 g of Yeast Extract (E-Merck, Germany), 5 g of sodium chloride (HiMedia, India), and 1 L distilled water. The pH was adjusted to 7.5 by using 1*N* hydrochloric acid and *N*/10 sodium hydroxide (approximately). The mass was stirred for 30 min for homogenization. About 15 g of agar-agar (Merck) was added to it and mixed thoroughly. About 25 mL of the media was mixed with nanocomposite dispersion to make 5:1 media: composite combination. Each combination was autoclaved at 120°C and 15 psi pressure for 15 min and then spread into petri plates under sterile condition at 40°C. The plates were allowed for solidification. Each composite was used to grow two different symbiotic bacterial stains namely Pseudomonas putida VM15A and Alcaligenes faecalis KK314. The pictures of the plates were taken initially, after 15 days and finally after 30 days.

Drug encapsulation efficiency (DEE) was analyzed by immersing the best membranes from each series into saturated Diltiazem solution and allowed the drug to diffuse inside the membranes (sorption). Reduced drug concentration in the solution was monitored through UV spectroscopic measurement at 236 nm (Perki Elmer Lambda 25 1.27) and comparing that with a standard calibration curve. A plot was generated with % drug absorbed against time interval to demonstrate DEE for each composite membrane.

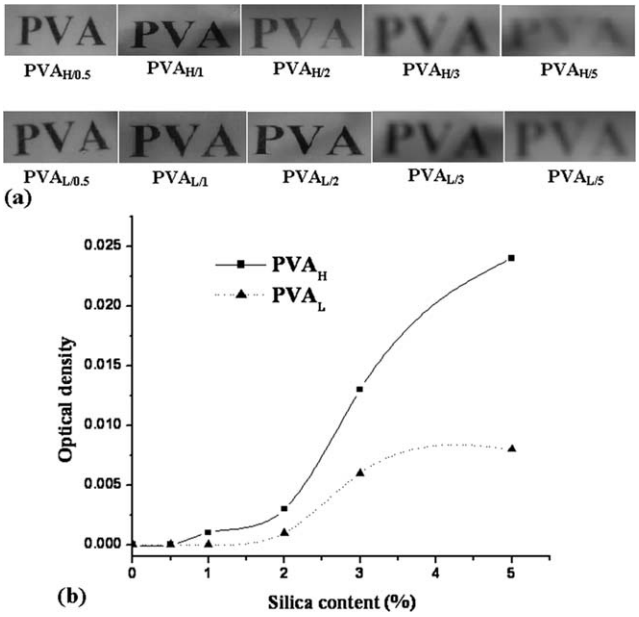

Figure 1. (a) Visual appearance and (b) optical densities of different PVA–silica hybrid membranes.

Transdermal release of diltiazem was analyzed in a Franz diffusion cell. Detailed description of the experiment has been reported in our earlier publication.[17,18]

RESULTS AND DISCUSSION

Visual Appearance and Optical Density Studies

Visual appearance of different PVA-nanosilica membranes were photographed (a digital camera from Sony, model: DSC-W180) and displayed in Figure 1(a). Pure PVA membranes were transparent (not shown here). Appearances of 0.5 wt % silica loaded membranes were also similar. High optical clarity probably indicates uniform nanosilica dispersion. But clarity gradually diminished on increasing nanosilica loading. It was because of the scattering of visual light from the edges of larger silica aggregates, which were formed at higher loading. In PVA$_L$ series, the membranes were apparently transparent till 2 wt % nanosilica content (PVA$_{L/2}$); whereas in PVA$_H$ series, similar transparency was retained only up to 1 wt % (PVA$_{H/1}$). Rests of the composites were highly translucent. In each case, optical density (OD) was measured at the visible region of the UV spectra to quantify optical clarity.[27] Results are plotted against silica loading in Figure 1(b). High OD indicates low visual clarity. The differences in OD of neat PVAs and at 0.5 and 1 wt % nanosilica contents between PVA$_H$ and PVA$_L$ composites were significantly high. Even OD of PVA$_{H/2}$ was much higher than PVA$_{L/2}$. Beyond 2 wt %, OD shoots off, especially for PVA$_H$ composites containing 3 and 5 wt % nanosilica. Never the less, OD tends to equilibrate beyond PVA$_{L/3}$ in PVA$_L$ series but it still showed sharp rising trend at similar silica content for PVA$_H$ membranes.

AFM, TEM, and EDX Silicon Mapping Analysis

AFM phase images of different PVA-nanosilica membranes are compared in Figure 2(a,c,e,f,h,j,k). Bright, near spherical features were harder silica domains and dark portions were soft PVA matrix. The grey portions denote interfacial regions

Applied Polymer SCIENCE

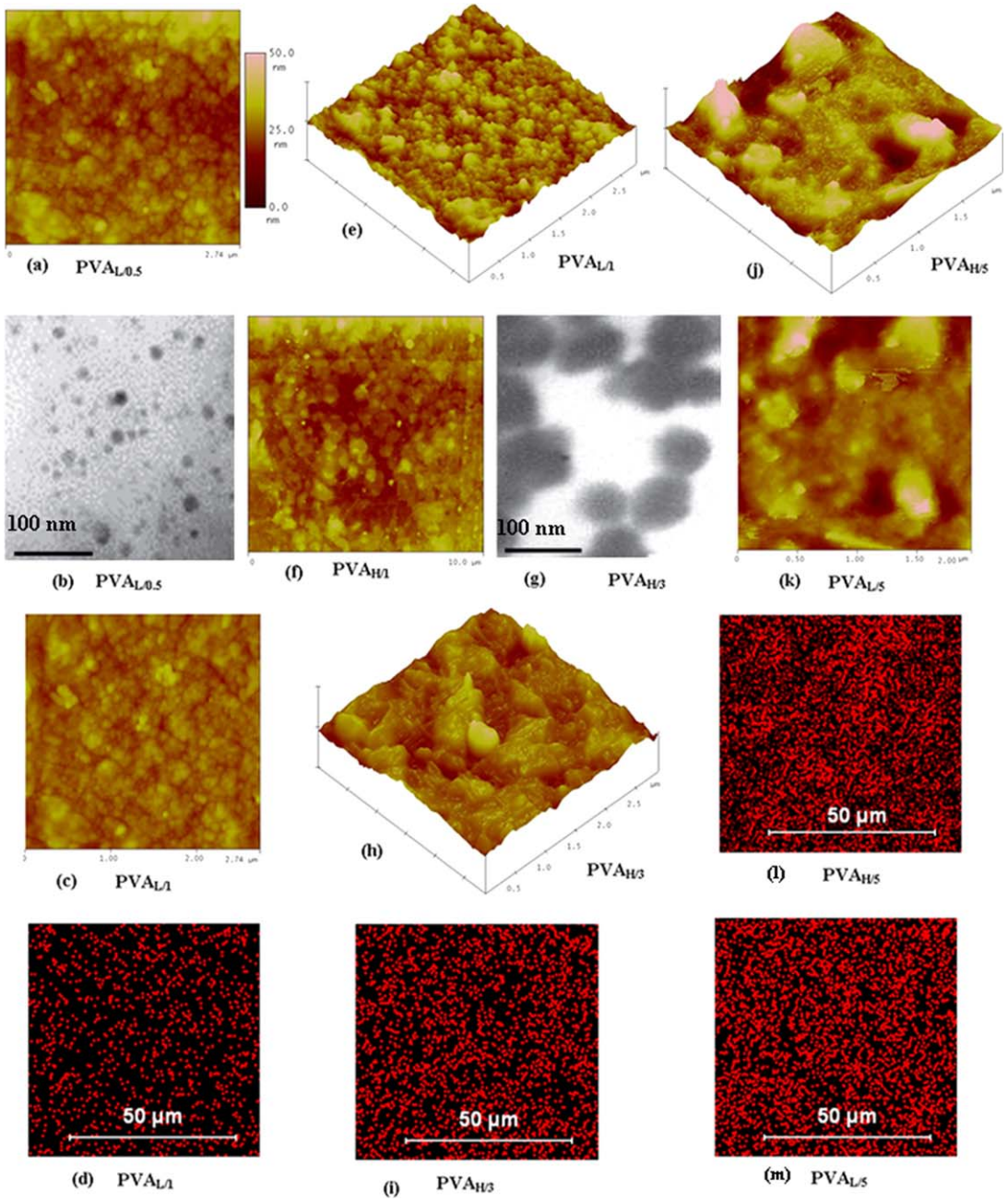

Figure 2. AFM, TEM, and EDX silicon mapping of representative PVA–silica hybrid membranes. [Color figure can be viewed in the online issue, which is available at wileyonlinelibrary.com.]

composed of PVA-coated silica domains. Uniform nanosilica dispersion with average diameter close to 21 nm was noted from the phase image of $PVA_{L/0.5}$ in Figure 2(a). The color gradients in major portions of this image elucidate excellent PVA_L–silica adhesion. Its TEM image in Figure 2(b) further elucidates similar dispersion status. Identical silica dispersion was also noticed in $PVA_{L/1}$ shown in Figure 2(c). EDX silicon mapping in Figure 2(d) further revealed that on larger scale. However, the size of the silica aggregates was slightly greater (average size 35 nm) than $PVA_{L/0.5}$. The 3d image showed that the silica aggregates were never too "bulging" from the average surface line that evidently reinstates better PVA–silica interaction at that composition [Figure 2(e)]. But, silica dispersion was never great in $PVA_{H/1}$ [Figure 2(f)] alike $PVA_{L/1}$, primarily because of lower hydrodynamic volume and adhesion than PVA_L.[28,29] The darker domains were proportionally higher in $PVA_{H/1}$ than in $PVA_{L/1}$, which evidently indicates presence of bare PVA_H fraction in $PVA_{H/1}$ as opposed to PVA_L in $PVA_{L/1}$. Average size of the silica aggregates accordingly rose to 85 nm, which was substantially higher than its size in $PVA_{L/1}$. Aggregates of even bigger sizes were noted in $PVA_{H/3}$ from its TEM image shown in Figure 2(g). Average width of such aggregates was 160 nm. Most of

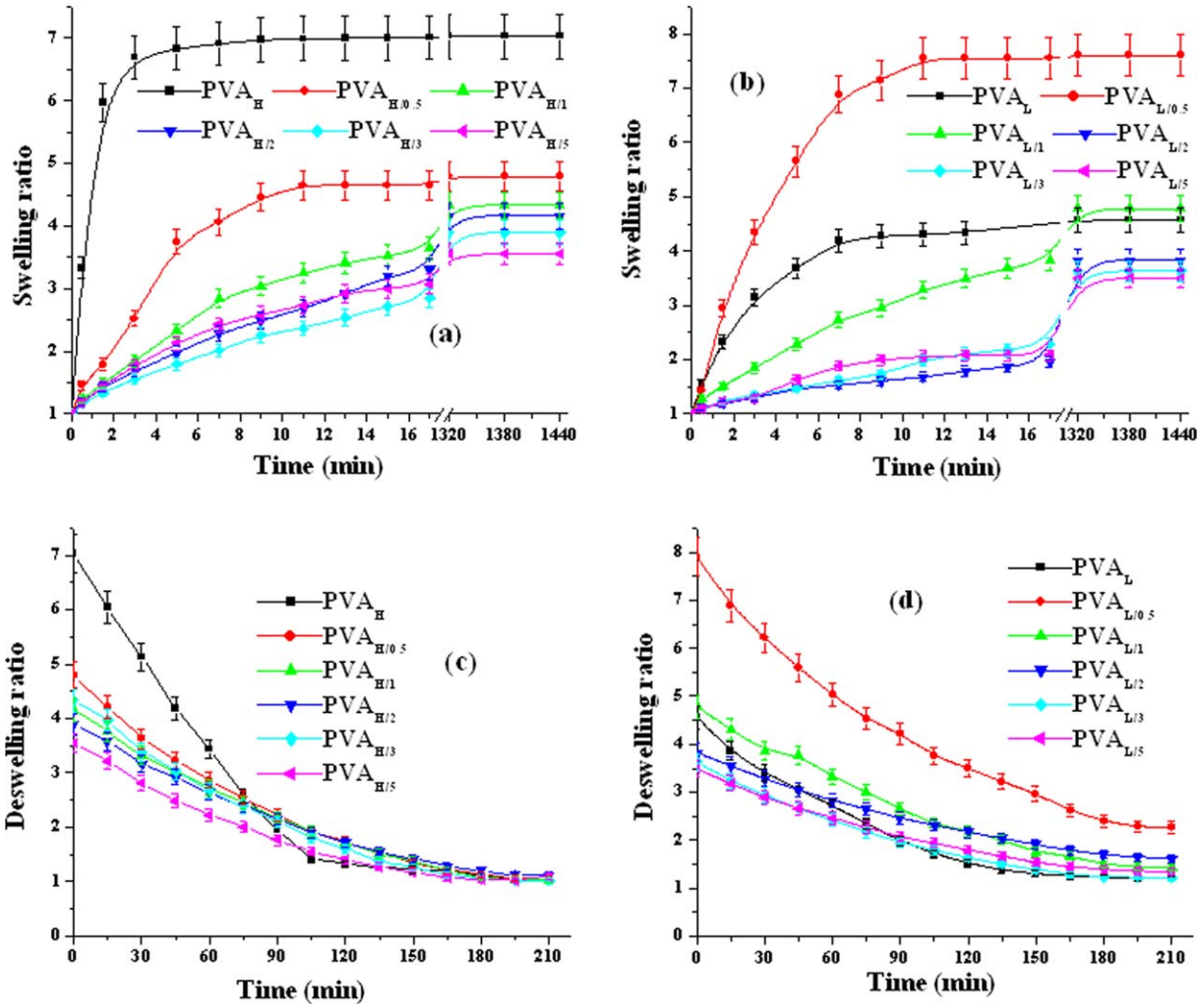

Figure 3. Swelling kinetics of (a) high and (b) low molecular weight and deswelling kinetics of (c) high and (d) low molecular weight hybrid PVA membranes. [Color figure can be viewed in the online issue, which is available at wileyonlinelibrary.com.]

them bulged out because of large surface energy difference [Figure 2(h)]. Those aggregates, on a bigger scale, were evident as local accumulation of silicon signals in EDX silicon mapping in Figure 2(i). The aggregate sizes further increased and were characteristically more bulging in $PVA_{H/5}$ [Figure 2(j)]. The situation was identical in $PVA_{L/5}$ [Figure 2(k)]. The aggregates form a continuous phase in them, called "cluster", with an average width more than 150 nm in $PVA_{H/5}$ and 120 nm in $PVA_{L/5}$. On bigger scale (EDX silicon mapping) those were evident as highly dense silicon signals. But, even in that situation, it was clear that silica domains were slightly denser and locally more aggregated in $PVA_{H/5}$ [Figure 2(l)] than in $PVA_{L/5}$ [Figure 2(m)].

Swelling De-Swelling Analysis

Swelling kinetics of neat PVA and its composite membranes are illustrated through Figure 3(a,b). The long swelling periods are accommodated by broken time axes in these figures. Neat PVA_H swelled faster than PVA_L and equilibrated within much shorter time interval (2 min) because of its higher hydroxyl content.[17] However, swelling was largely affected in the presence of nanosilica. In PVA_H series, neat PVA_H was the fastest swelling membrane followed by $PVA_{H/0.5}$, $PVA_{H/1}$, $PVA_{H/2}$, $PVA_{H/3}$, and $PVA_{H/5}$ [Figure 3(a)]. Conversely in PVA_L series, $PVA_{L/0.5}$ was the fastest followed by PVA_L, $PVA_{L/1}$, $PVA_{L/2}$, $PVA_{L/3}$, and $PVA_{L/5}$ [Figure 3(b)]. But, despite faster swelling, net swelling ratio was still higher in $PVA_{L/1}$ than in PVA_L. Low swelling efficacy of PVA_H composites was because of more silica aggregation and loss in PVA_H volume fraction. Conversely, greatly improved swelling behavior of $PVA_{L/0.5}$ was because of huge water attraction by the silanol groups of uniformly dispersed nanosilica particles. In $PVA_{L/1}$, PVA–silica adhesion was much stronger than $PVA_{L/0.5}$ because of optimal silica loading, which strongly retarded its swelling rate initially by immobilizing the PVA_L segments but it continued and finally the nanocomposite absorbed higher equilibrium water through interaction with silanol groups. But beyond 1 wt % loading, more silica aggregation and loss in PVA_L volume concentration led to even lower swelling states in PVA_L composites. The aggregates formed strong hydrophobic silica overcoat and produced high resistance against penetration of water molecules.

Applied Polymer SCIENCE

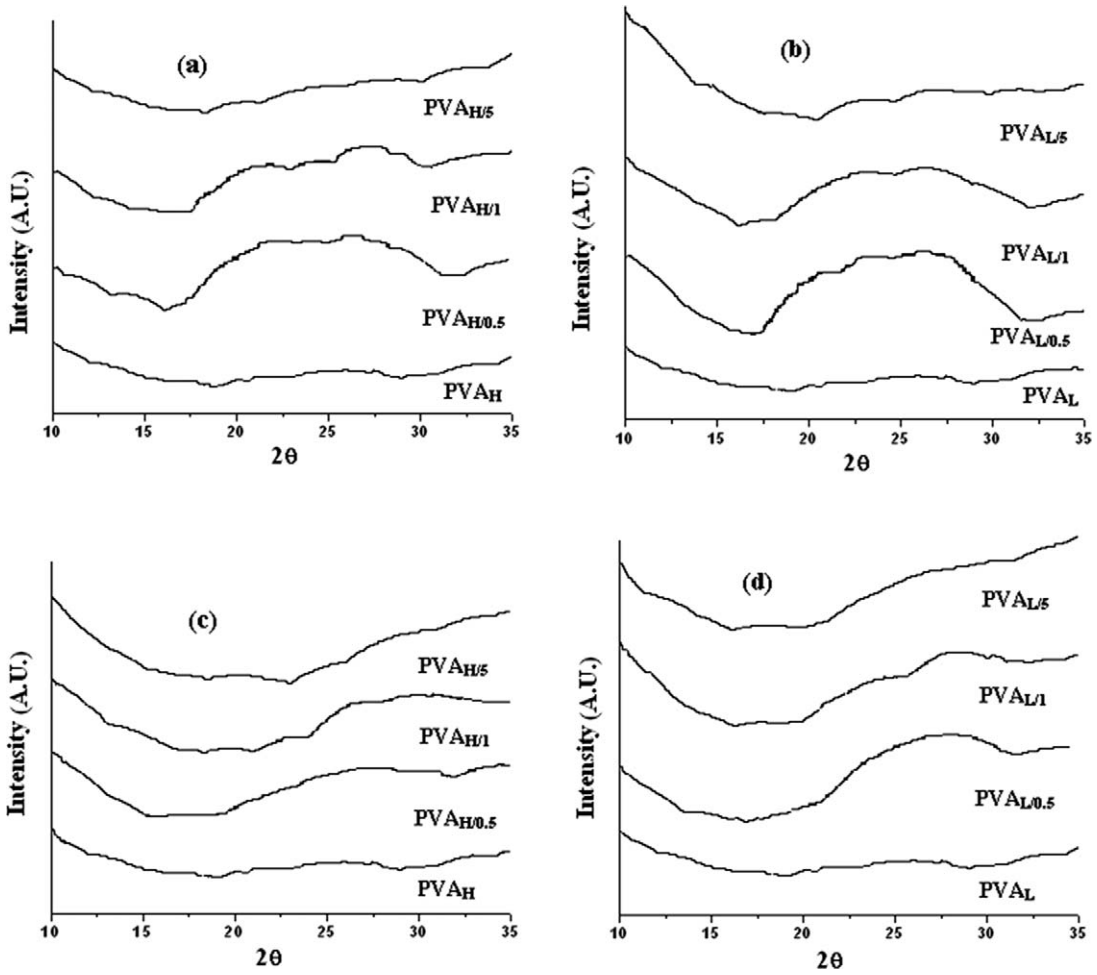

Figure 4. XRD spectra of (a) PVA_H and (b) PVA_L hybrid membranes in dry state and (c) PVA_H and (d) PVA_L in swelled state.

The de-swelling kinetics is displayed in Figure 3(c,d). All de-swelling profiles were exponential and finally led to constant water content value called "equilibrium water". The profile clearly showed that the membranes that absorbed higher amount of water also released that at a faster rate in order to get rid of its high internal pressure. Neat PVA_H and $PVA_{L/0.5}$ perfectly demonstrated those behaviors. However, in PVA_H series, the de-swelling and equilibrium water content closely varied between different composite membranes [Figure 3(c)] but in PVA_L series, the equilibrium water content in different membranes was more discernible [Figure 3(d)]. $PVA_{L/0.5}$ retained maximum equilibrium water despite of its high swelling pressure followed by $PVA_{L/2}$, $PVA_{L/1}$, $PVA_{L/3}$, $PVA_{L/5}$, and PVA_L. Alike PVA_H, PVA_L also retained minimum equilibrium water in the series.

Crystallinity Analysis through XRD

Wide angle X-ray diffractograms of neat PVAs and their composite membranes are shown in Figure 4. Dry PVA_H [Figure 4(a)] and PVA_L membranes [Figure 4(b)] did not show any diffraction peaks.[17] However, the composites containing 0.5 and 1 wt % nanosilica of both PVA_H and PVA_L series exhibited strong diffraction band between 2θ = 16.5–32° but not so at 5 wt %. The crystalline band in hybrid composites eventually composed of two super imposed peaks—the first between 2θ =18–20°[30] denoting diffraction from crystalline PVA lamella and the second between 2θ = 22–30°[31,32]denoting diffraction from nanosilica particles. Both at 0.5 and 1 wt % nanosilica content, PVA_L displayed slightly higher band area than PVA_H (25% higher at 0.5 wt % and 18% higher at 1 wt % nanosilica contents) possibly because of the presence of more crystalline fraction in PVA_L composites than PVA_H at similar silica contents. The reason could be better nanosilica distribution in PVA_L by occupying its available free volume. At 5 wt %, the crystallinity vanishes because of (i) massive silica aggregation and (ii) high equilibrium water content reducing the size of PVA crystal lamella.

Solid State ^{13}C NMR Analysis

Solid state ^{13}C NMR spectra of neat PVA_H and PVA_L and their hybrid membranes are displayed in Figure 5. The characteristic peaks are reported in the figure itself. Chemical shift in each spectrum can be divided into two regions. Resonance at low field region between 65 and 80 ppm was assigned to methine carbon and at high field region between 44 and 54 ppm was for

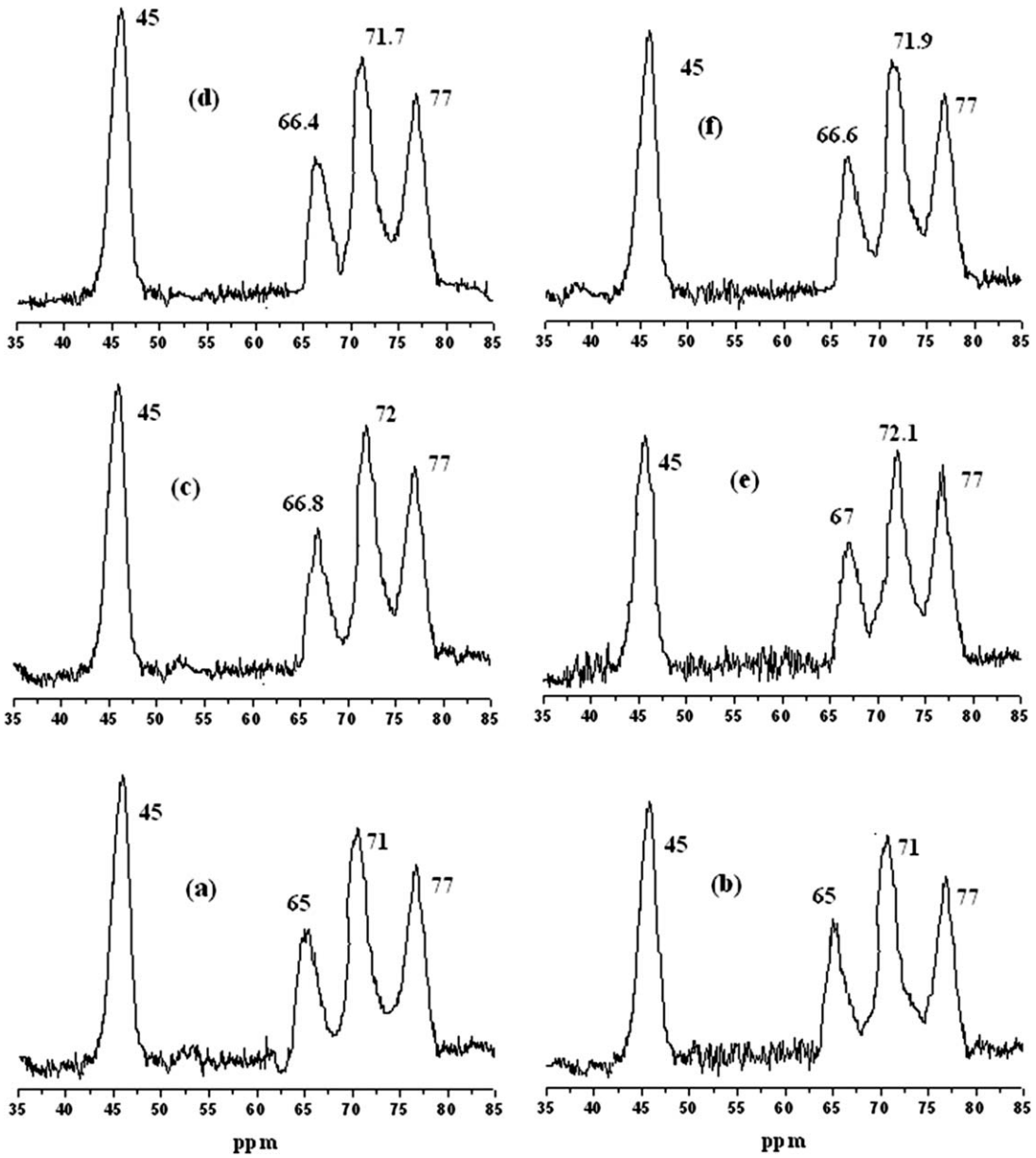

Figure 5. Solid state ^{13}CNMR of (a) PVA_H, (b) PVA_L, (c) $PVA_{H/1}$, (d) $PVA_{H/3}$, (e) $PVA_{L/1}$, and (f) $PVA_{L/3}$ hybrid membranes.

methylene carbon. The low field region for both PVA_H [Figure 5(a)] and PVA_L [Figure 5(b)] showed three peak (triad) resonances at δ = 77, 71, and 65 ppm because of tacticity of methine carbon (Scheme 2).[33,34] According to Tearo,[34] in solid state, down field shift of these triad peaks into different δ values denote different extent of supramolecular interactions in these components. The peak at 77 ppm represents mm triad with two intramolecular hydrogen bonds whereas the peak at 71 ppm was for mr triad with one intramolecular hydrogen bond and finally the peak at 65 ppm was for rr triads without any intramolecular hydrogen bonds. In $PVA_{H/1}$ [Figure 5(c)] the three absorption peaks were observed at δ = 66.8, 72, and 77 ppm which indicate strong intermolecular hydrogen bonding (interaction) between hydroxyl groups of PVA and silanol groups of nanosilica in mr and rr triads. Here the electron density of methine carbon was transferred to nanosilica phase as indicated by the downfield shift of the carbon peak resonances. Logically, there was no shift of mm triad peaks as there was no scope for intermolecular hydrogen bonding (Scheme 2). But for rr triads shifting of peak was nearly two times than mr triad because of greater extent (two versus one hydroxyl groups) of intermolecular interaction. In $PVA_{H/3}$ [Figure 5(d)] the shift was not prominent alike $PVA_{H/1}$ because of lesser interaction between nanosilica and PVA_H because at higher concentration, silica formed larger aggregates utilizing most of its silanol groups. Similar differences were also observed between $PVA_{L/1}$ [Figure 5(e)] and $PVA_{L/3}$ [Figure 5(f)]. However, shift of concerned peaks were slightly higher in $PVA_{L/1}$ and $PVA_{L/3}$ than in $PVA_{H/1}$ and $PVA_{H/3}$ due to stronger PVA–silica

Applied Polymer SCIENCE

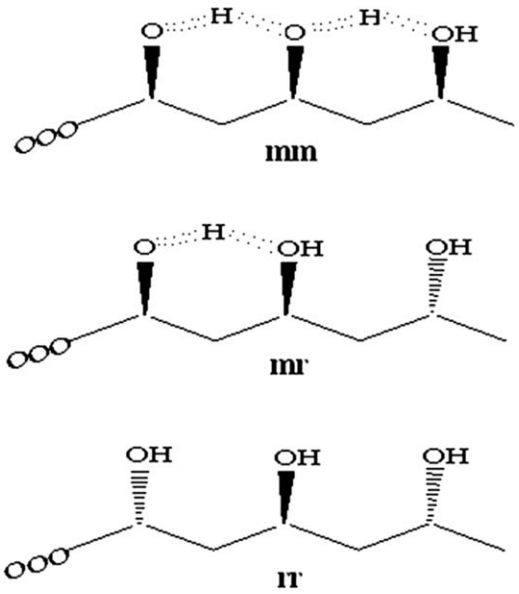

Scheme 2. Methine carbons of PVA in mm, mr, and rr triads.

interaction. But, at all instances, methylene carbon resonance at $\delta = 45$ ppm does not shift as very little electron density shift was expected for that carbon.

Dry State Mechanical Property Analysis

Mechanical properties of dry PVA/silica membranes at different silica concentrations are compared in Figure 6(a,b). Tensile strength of dry PVA_H hybrids increased up to 1 wt % nanosilica content [Figure 6(a)]; whereas it was up to 2 wt % in case of PVA_L [Figure 6(b)], even though, $PVA_{L/2}$ was expected to have some local silica aggregation. Beyond that, the tensile strength went down. Similarly, maximum modulus was shown by $PVA_{H/1}$ in PVA_H series and $PVA_{L/2}$ in PVA_L series. At low loading, the rise in strength and modulus was because of uniform nanosilica dispersion and consequent rise in dry state crystallinity. However, drop in tensile strength and moduli demonstrated deleterious effects of large silica aggregates that reduced PVA–silica interaction beyond 1 or 2 wt %, as the case with PVA_H or PVA_L. Composites of PVA_L were stronger (superior tensile strength and modulus) at each silica loading than PVA_H. The reason could be slightly higher percentage crystallinity at low silica concentration than PVA_H whereas higher PVA_L–silica interaction still retained at its higher loading levels than equivalent PVA_H composites. Elongation at break had unexpectedly increased along with tensile strength and moduli at low silica content and then sharply went down. The closely adhered nanosilica particles to PVA assisted for dissipating the impressed mechanical stress on the membranes at low concentration which,

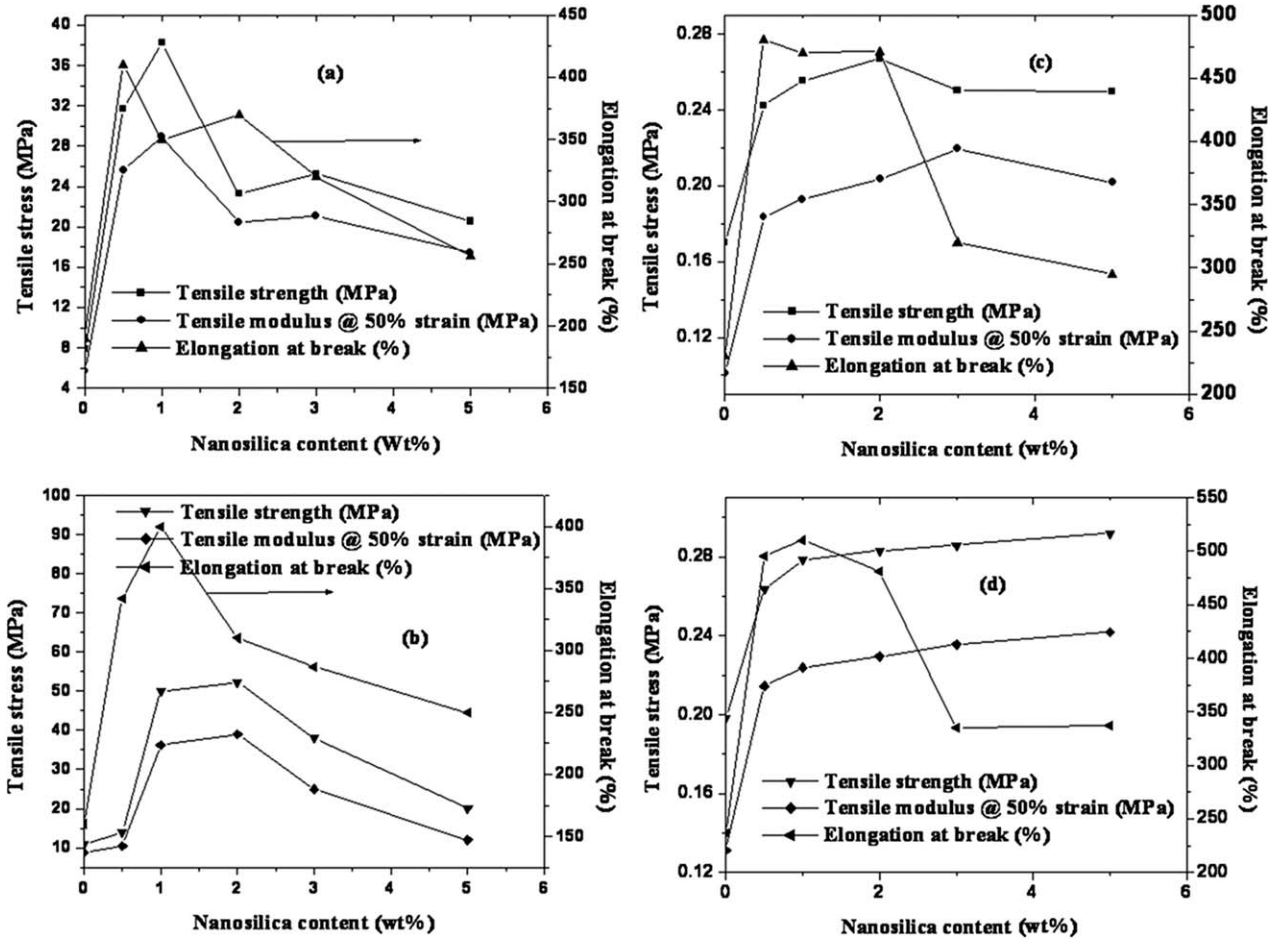

Figure 6. Mechanical property of (a) PVA_H and (b) PVA_L hybrid membranes in dry state and (c) PVA_H and (d) PVA_L hybrid membranes in swelled state.

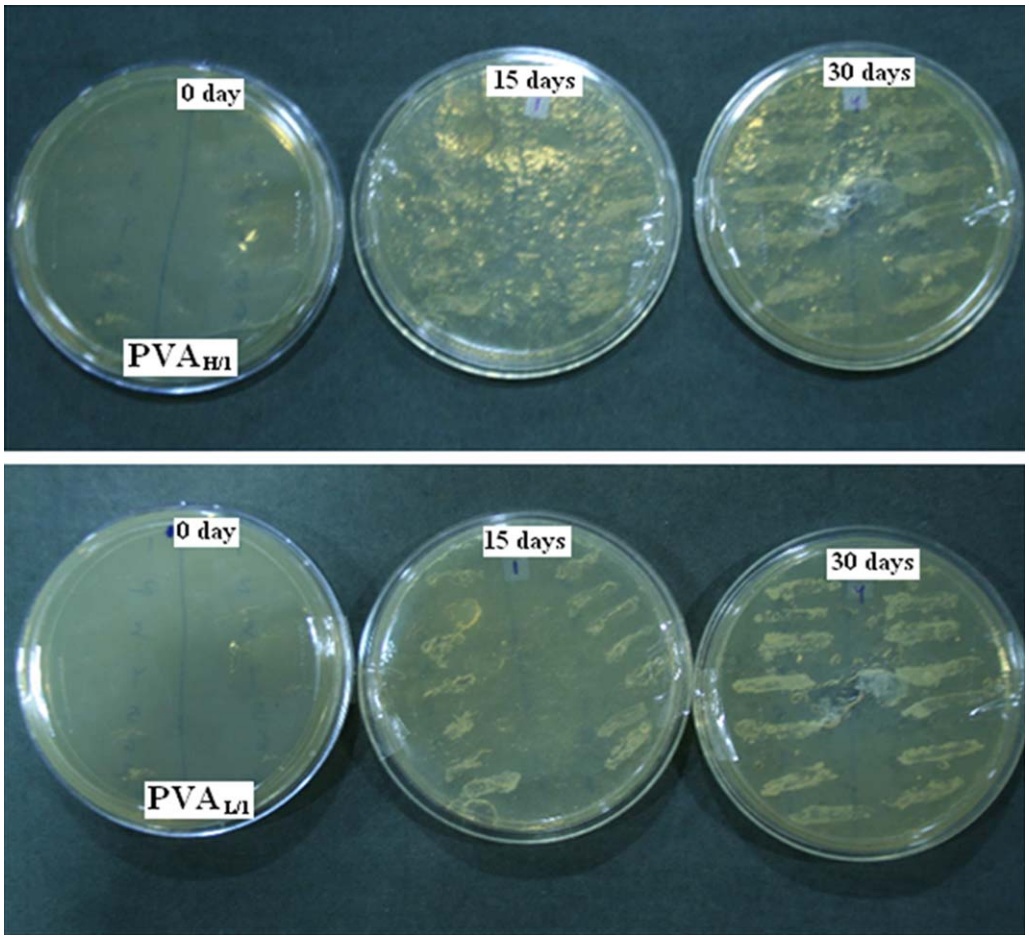

Figure 7. Microbial growth potentials of pseudomonas putida VM15A (left) and alcaligenes faecalis KK314 (right) after 0, 15, 30 days of $PVA_{L/1}$ and $PVA_{H/1}$. [Color figure can be viewed in the online issue, which is available at wileyonlinelibrary.com.]

had failed since the bigger silica aggregates acted as stress concentrators at high concentration.

Postswelling XRD and Mechanical Property Analysis after Swelling

On swelling, no PVA diffraction peaks appeared in PVA_H and PVA_L [Figure 4(c,d)] as was the case observed with freeze-thaw treated PVAs.[17] Rather, the PVA crystalline band in the hybrids (at 0.5 and 1 wt % silica content) disappeared because of dissolution of the crystalline lamella by excess water molecules. However, crystalline band of nanosilica (2θ = 22–30°) was still retained as it was less affected than PVA molecules on swelling.

Presence of excess water reduced both tensile strength and modulus from its dry state but had slightly increased net elongations because of plasticization. In the swelled state, both tensile strength and modulus increased up to $PVA_{H/2}$ from the neat in PVA_H series but those were asymptotic in PVA_L composites [Figure 6(c,d)]. At low silica content, the finer particles helped in better stress transfer, which raised the tensile strength till $PVA_{H/2}$ but similar effect was retained in all PVA_L composites owing to stronger PVA_L–silica interfaces.

Biocompatibility Study

Contextually, $PVA_{H/1}$ from PVA_H series and $PVA_{L/1}$ from PVA_L series were selected to check the effect of nanosilica on microbial growth potential, assumed as a measure of their biocompatibility. As shown in Figure 7, the composite plates were divided in two parts to detect growth volume of individual stains—the left side contains Pseudomonas putida VM15A and the right side contains Alcaligenes faecalis KK314.[35] It was seen that $PVA_{H/1}$ produced higher growth volume than $PVA_{L/1}$ at all stages (15 and 30 days) under similar condition in spite of the fact that it was tough to break the long and coiled molecular segments of high molecular weight mass than the low molecular weight mass (free and flexible chain segment). Low percentage crystallinity of $PVA_{H/1}$ facilitated better microbial access than $PVA_{L/1}$ and finally have shown higher growth potential than $PVA_{L/1}$. Interestingly, presence of nanosilica did not infuse any adverse effect towards biocompatibility yet produced excellent physico-mechanicals apposite for patch therapy.

DEE and Diltiazem Release Kinetics Study

DEE between $PVA_{H/1}$ and $PVA_{L/1}$ membranes are compared in Figure 8(a). Drug encapsulation by $PVA_{L/1}$ was notably much

Applied Polymer SCIENCE

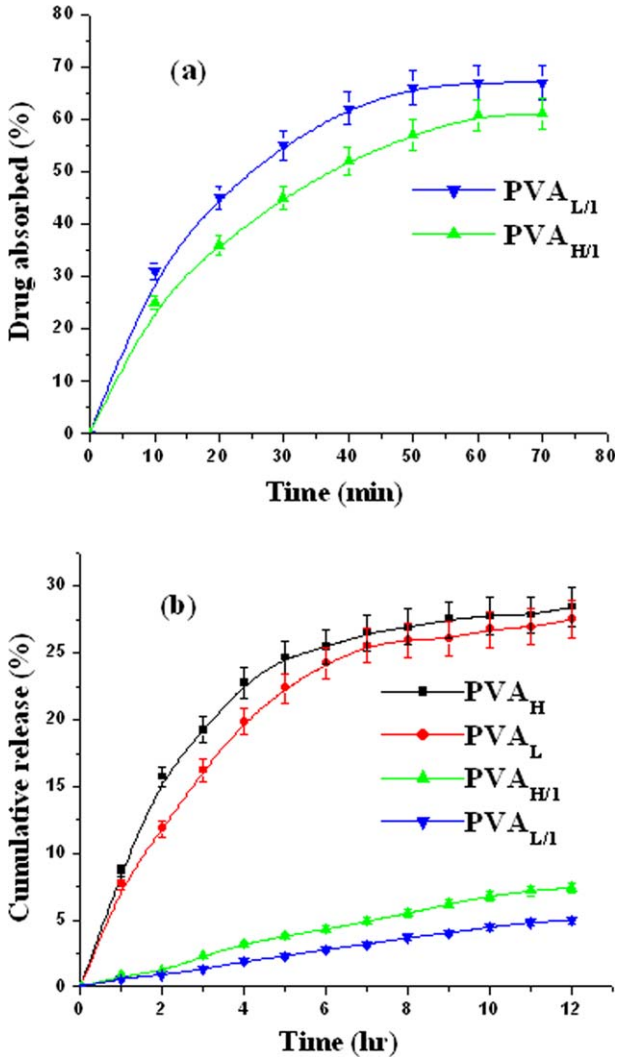

Figure 8. (a) DEE of $PVA_{L/1}$ and $PVA_{H/1}$, (b) drug release kinetics of PVA_H, PVA_L, $PVA_{L/1}$, and $PVA_{H/1}$ membranes. [Color figure can be viewed in the online issue, which is available at wileyonlinelibrary.com.]

higher than $PVA_{H/1}$ because of greater interaction of the Diltiazem molecules with more finely distributed nanosilica particles. It eventually stabilized the drug molecules into the matrix cavity by supramolecular interaction. Moreover, high swelling efficacy of $PVA_{L/1}$ promoted faster Diltiazem uptake than $PVA_{H/1}$. The data show, within first 10 min, that 31% of the drug was absorbed by $PVA_{L/1}$, whereas only 25% by $PVA_{H/1}$ and finally saturation achieved within 55 min in $PVA_{L/1}$ and 61 min in $PVA_{H/1}$. The equilibrium DEE of $PVA_{L/1}$ was 67% and it was 61% for $PVA_{H/1}$.

Diltiazem release kinetics from $PVA_{H/1}$, $PVA_{L/1}$ and neat PVAs are compared in Figure 8(b). The kinetics follows the power law model, expressed in the following equation[17,36,37]:

$$M_t/M_\alpha = kt^n \quad (1)$$

Here M_t/M_∞ denotes fractional release of Diltiazem at time *t*. *k* and *n* are constants related to diffusion coefficient and specific drug transport mechanism. The *k* and *n* values for all four membranes are reported in Table I. Both PVA_H and PVA_L showed true bursting features, i.e. high *k* values of 10.83 and 8.79 and *n* values of 0.43 and 0.49, corroborating with their faster swelling kinetics. Generally, $n \leq 0.5$ indicates Fickian diffusion controlled release, whereas $n \geq 0.5$ indicates non-Fickian, i.e. mixed behavior of Fickian and relaxation or case II transport-based release. However, $n \geq 1$ fully stands for relaxation controlled release.[38] Both PVAs showed Fickian release owing to their poor mechanical strength. PVA_L was shed slower than PVA_H because of its slightly higher strength and viscosity.[28,29] Addition of nanosilica had significantly reduced elution rate (Scheme 3) and abolished the bursting feature. Both $PVA_{H/1}$ and $PVA_{L/1}$ showed prominent case II transport (*n* values are close to 1)-based elution. Higher encapsulation of the drug molecules than neat had effected into slow and more controlled release of the same. However, the release was more slow and sustained in $PVA_{L/1}$ than in $PVA_{H/1}$ because of greater drug-nanosilica-PVA_L interaction and higher crystallinity. After 12 hrs, $PVA_{L/1}$ released less than 5% of the encapsulated drug, whereas it was 7.4% in case of $PVA_{H/1}$. Those results suggested that either the initial drug loading could be adjusted or multiple membranes could be used to deliver optimum drug concentration in the blood for therapeutic action.

CONCLUSION

Molecular weight changes of PVA had evidently produced some significant physical and mechanical property differences between the membranes. The key properties like mechanical and swelling were strongly affected because of abrupt change in silica morphology as because, at higher silica content, the inorganic phase approached more towards the surface and produced a strong hydrophobic coat. Better property balance was obtained at low

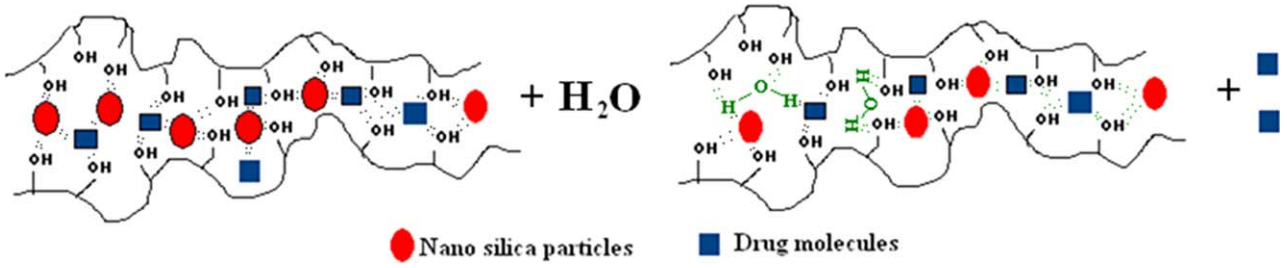

Scheme 3. Probable encapsulation and release mechanism of diltiazem through PVA *ex situ* nanosilica membranes. [Color figure can be viewed in the online issue, which is available at wileyonlinelibrary.com.]

silica content, especially at 1 wt %. Evidently, $PVA_{L/1}$ was more strong and extendible than $PVA_{H/1}$ because of higher PVA–silica interaction leading to higher percentage crystallinity. On swelling, strength and modulus was still higher because of stronger PVA_L–silica interfaces. However, $PVA_{L/1}$ was slightly less biocompatible than $PVA_{H/1}$, which, in other way, was advantageous as it ensured its better endurance than $PVA_{H/1}$. Diltiazem release was slower and free of burst through $PVA_{L/1}$ because of its higher DEE than $PVA_{H/1}$. For both membranes, the cumulative release data advised as either adjustment in initial drug loading in a single patch or use of multiple patches with distributed drug load to achieve equilibrium concentration for therapeutic action.

REFERENCES

1. Jaspart, S.; Bertholet, P.; Piel, G.; Dogne, J.M.; Delattre, L.; Evrard, B. *Euro. J. Pharm. Biopharm.* **2007**, *65*, 47.
2. Moskowitz, J.S.; Blaisse, M.R.; Samuel, R.E.; Hsu, H.P.; Harris, M.B.; Martin, S.D.; Lee, J.C.; Spector, M.; Hammond, P.T. *Biomaterials.* **2010**, *31*, 6019.
3. Srinivas, P.; Sunitha, M.; Babu, D. S. R.; Sadanandam, M. *Int. J. Pharm. Sci.* **2011**, *3*, 1152.
4. Hamidi, M.; Azadi, A.; Rafiei, P. *Adv. Drug Deliv. Rev.* **2008**, *60*, 1638.
5. Contreras-Garcia, A.; Bucio, E.; Concheiro, A.; Alvarez-Lorenzo, C. *J Bioact. Comp. Polym.* **2011**, *26*, 405.
6. Kingsley, J. D.; Dou, H.; Morehead, J.; Rabinow, B.; Gendelman, H. E.; Destache, C. J. *J. Neuroimmune Pharmacol.* **2003**, *1*, 340.
7. Adnadjevic, B.; Jovanovic, J.; Drakulic, B. *Thermochimica Acta.* **2007**, *466*, 38.
8. Brigger, I.; Dubernet, C.; Couvreur, P. *Adv. Drug. Deliv. Rev.* **2002**, *54*, 631.
9. Peng, K. T.; Chen, C. F.; Chu, I. M.; Li, Y. M.; Hsu, W. H.; Hsu, R. W.; Chang, P. J. *Biomaterials.* **2010**, *31*, 5227.
10. Ji, Q. X.; Deng, J.; Xing, X. M.; Yuan, C. Q.; Yu, X. B.; Xu, Q. C.; Yue, J. *Carbohy. Polym.* **2010**, *82*, 1153.
11. Siddaramaiah.; Kumar, P.; Divya, K. H.; Mhemavathi, B. T.; Manjula, D. S. *J. Macromol. SCI. A.* **2006**, *43*, 601.
12. Prisant, L. M.; Elliott, W. J. *Clinical Pharmacokinetics,* **2003**, *44*, 931.
13. Puche, J. J.; Garcia-Coret, M. J.; Villalba, F. L.; Mahmoud, I. A.; Roig, J. V. *A comparative study Cirugia Espanola (English Edition).* **2010**, *87*, 224.
14. Kim. S.; Kim, J. H.; Jeon, O.; Kwon, I. C.; Park, K. *Euro. J. Pharm. Biopharm.* **2009**, *71*, 420.
15. Kulkarni, R.V.; Sa, B. *J. Bioact. Comp. Polym.* **2009**, *24*, 368.
16. De-Giglio, E.; Cafagna, D.; Giangregorio, M. M.; Domingos, M.; Mattioli-Belmonte, M.; Cometa, S. *J. Bioact. Comp. Polym.* **2011**, *26*, 420.
17. Bhunia, T.; Bhowmik, M.; Chattopadhyay, D.; Bandyopadhyay, A. *J. Appl. Polym. Sci.* **2012**, *124*, E177.
18. Bhunia, T.; Goswami, L.; Chattopadhyay, D.; Bandyopadhyay, A. *Nucl. Instrum. Meth. B.* **2011**, *269*, 1822.
19. Deng, L.; Hagg, M. B. *J. Membrane Sci.* **2010**, *363*, 295.
20. Yang, W. H.; Smolen, V. F.; Peppas, N. A. *J. Membrane Sci.* **1981**, *9*, 53.
21. Bandyopadhyay, A.; De Sarkar, M.; Bhowmick, A. K. *J. Polym. Sci. Part B: Polym. Phys.* **2005**, *43*, 2399.
22. Spitalsky, Z.; Tasis, D.; Papagelis, K.; Galiotis, C. *Prog. Polym. Sci.* **2010**, *35*, 357.
23. Yang, C. C. *J. Membrane Sci.* **2007**, *288*, 51.
24. Rao, Y. Q. *Polymer.* **2007**, *48*, 5369.
25. Mishra, T. K.; Kumar, A.; Verma, V.; Pandey, K. N.; Kumar, V. *Compos. Sci. Technol.* **2012**, *72*, 1627.
26. Bandyopadhyay, A.; De Sarkar, M.; Bhowmick, A. K. *J. Mater. Sci.* **2005**, *40*, 5233.
27. Sengupta, R.; Bandyopadhyay, A.; Sabharwal, S.; Chaki, T. K.; Bhowmick, A. K. *Polymer.* **2005**, *46*, 3343.
28. Nasim, T.; Bandyopadhyay, A. *Sep. Purif. Technol.* **2012**, *88*, 87.
29. Bhunia, T.; Chattopadhyay, D.; Bandyopadhyay, A. *J. Sol Gel Sci. Technol.* **2011**, *59*, 260.
30. Mari. Y.; Tokura, H.; Yoshikawa, M. *J. Mater. Sci.* **1997**, *32*, 491.
31. Thuadaij, N.; Nuntiya A. *Chiang Mai J. Sci.* **2008**, *35*, 206.
32. Nakane, K.; Yamashita, T.; Iwakura, K. *J. Appl. Polym. Sci.* **1999**, *74*, 133.
33. Ketels, H.; Haan, J. D.; Aerdts, A. *Polymer* **1990**, *31*, 1419.
34. Tearo, T.; Maeda, S.; Saika, A. *Maromolecules* **1983**, *16*, 1535.
35. Riaz, U.; Ashraf, S. M.; Sharma, H. O. *Polym. Degrad. Stabil.* **2011**, *96*, 33
36. Peppas, N. A.; Bures, P.; Leobandung, W. *Euro. J. Pharm. Biopharm.* **2000**, *50*, 27.
37. Lin, C. L.; Metters, A. T. *Adv. Drug Deliv. Rev.* **2006**, *58*, 1379.
38. Peppas, N. A.; Khare, A. R. *Biomaterials* **1995**, *16*, 559.